A NUMERICAL INVESTIGATION OF THE EFFECTS OF ROTATION ON TURBULENT PIPE FLOWS

C. Brehm, J. Davis, S. Ganju, and S. Bailey

Mechanical Engineering Department University of Kentucky 151 Ralph G. Anderson Building Lexington, KY 40506-0503, USA email: christoph.brehm@uky.edu

ABSTRACT

In past experiments, simulations and theoretical analysis, rotation has been shown to dramatically effect the characteristics of turbulent flows, such as causing the mean velocity profile to appear laminar, leading to an overall drag reduction, as well as affecting the Reynolds stress tensor. The axially rotating pipe is an exemplary prototypical model problem that exhibits these complex turbulent flow physics. For this flow, the rotation of the pipe causes a region of turbulence suppression which is particularly sensitive to the rotation rate and Reynolds number. The physical mechanisms causing turbulence suppression are currently not well-understood, and a deeper understanding of these mechanisms is of great value for many practical examples involving swirling or rotating flows, such as swirl generators, wing-tip vortices, axial compressors, hurricanes, etc.

In this work, Direct Numerical Simulations (DNS) of rotating turbulent pipe flows are conducted at moderate Reynolds numbers (Re=5300, 11,700, 19,000) and rotation numbers of N=0 to 3. The main objectives of this work are to firstly quantify turbulence suppression for rotating turbulent pipe flows at different Reynolds numbers as well as study the effects of rotation on turbulence by analyzing the characteristics of the Reynolds stress tensor and the production and dissipation terms of the turbulence budgets.

1 Brief Introduction

The current research is concerned with axially rotating pipe flow as schematically illustrated in Fig. 1. In this flow, the axis of rotation is parallel to the mean flow direction and, therefore, for the laminar case the axial mean flow is not directly affected by the rotation. Hence, the parabolic mean flow profile observed in laminar non-rotating pipes also describes the axial (laminar) velocity profile for the rotating case. The axially rotating pipe can be described by two non-dimensional parameters, i.e., the Reynolds number Re = UD/v based on the mean bulk flow velocity U, the pipe diameter D, and the kinematic viscosity v as well as the rotation number $N = V_w/U$ of the pipe, which is sometimes also referred to as swirl rate. The rotation number characterizes the angular velocity Ω through the azimuthal velocity of the pipe inner wall, $V_{\theta}(r=R) = \Omega D/2$ (in nonrotating reference frame).

The turbulent flow through a rotating pipe is an excellent prototypical case to investigate the physical mech-

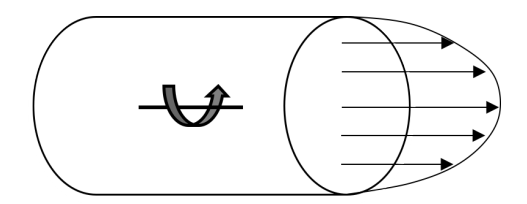


Figure 1. Schematic of axially rotating pipe flow.

anisms causing relaminarization of rotating flows. While models, such as RANS and wall-resolved LES, fail to accurately reproduce the flow physics involved in turbulence suppression, DNS can be used to effectively study rotation effects on turbulent structures. The reader may refer to Ashton *et al.* (2019) comparing several RANS models with the DNS data presented here. Existing DNS studies of rotating pipe flows have been restricted to relatively low Reynolds numbers and a strong dependence on rotation number has been observed. Thus, one of the goals of the current work is to provide detailed DNS data at large Reynolds numbers.

White (1964) was among the first to conduct experiments on rotating pipe flow and observed a reduction of up to 40% in pressure loss for very high rotation numbers and attributed this to suppression of transport in the radial direction. Kikuyama et al. (1983) experimentally observed that an initially turbulent flow can be seemingly relaminarized with sufficiently large N while initially laminar flow was found to be destabilized by the rotation. Imao et al. (1996) confirmed a reduction of turbulence intensity with increasing rotation rate and verified a relationship between the reduced mixing length and the Richardson number. Most recently, Facciolo et al. (2007) obtained good agreement of the mean velocity distribution with the scaling provided by Oberlack (1999) who used the Lie group approach presented in Oberlack (2001) to derive new scaling laws for high-Re rotating and non-rotating turbulent pipe flows.

In comparison to the (spanwise) rotating channel flow, very few numerical studies have been conducted for the rotating circular pipe flow. All prior DNS studies were performed for $Re \leq 7,400$ and typically at relatively low N, where some type of turbulence suppression seemingly occurred, but not full relaminarization. Orlandi & Fatica (1997) conducted the most extensive set of DNS studies, studying rotation numbers up to N=2 at Re=4,900 (later even up to N=10 in Orlandi & Ebstein (2000)). A type of

relaminarization that is not well understood at the moment has been observed for these rotation rates. In the reported relaminarization process the mean streamwise velocity profile is approaching the laminar Poiseuille profile. While Nishibori et al. (1987) and Reich & Beer (1989) explained the changes in the mean flow and the turbulence by drawing a general connection to the centrifugal force, Orlandi & Fatica (1997) concluded that this occurred through modification of the near wall flow structures. Their numerical simulations only qualitatively captured the drag and turbulence reductions observed in the experiments (by Murakami & Kikuyama (1980); Kikuyama et al. (1983); Reich & Beer (1989)). They justified the difference between the experimental and DNS data sets by referring to the uncertainty of the flow conditions in the experiments and it was speculated that the streamwise location where the measurements were taken was not far enough downstream to observe fullydeveloped conditions.

Feiz *et al.* (2005) conducted DNS for fully developed turbulent flows in stationary and axially rotating pipes. In this study, the effect of the Reynolds number was investigated by considering two different Reynolds numbers Re = 4,900 and Re = 7,400 as well as rotation numbers up to N = 2. It was noted that the axial mean velocity profiles for Re = 7,400 have lower values than for Re = 4,900. The tangential mean velocity profiles appear to be very similar for both Reynolds numbers. They also conducted LES at Re = 20,000 and reported that the decrease of the skin friction factor with N is more pronounced for larger Re.

The current paper will proceed as follows: Section 2 provides an overview of the simulation setup and numerical approach. The effects of rotation on the turbulent meanflow are discussed in Section 3. Section 4 quantifies turbulence suppression in rotating flows. The changes in the structure of the Reynolds stress tensor are discussed in Section 5 and, finally, the analysis of the production and dissipation terms in Section 6 provide some clues about the suppression of turbulence in the rotating flow.

2 SIMULATION SETUP

In order to study the physical phenomena occurring in a rotating turbulent flow we conducted DNS at three Reynolds numbers, i.e., Re = 5,300, 11,700, and 19,000.For these simulations we assume fully-developed turbulent flow and periodic boundaries in the streamwise direction. The incompressible Navier-Stokes equations are solved in a reference frame rotating with the pipe walls where the centrifugal and Coriolis forces were added as source terms. Sufficient temporal and spatial resolution is required to thoroughly study the intricate nature of turbulence and the relevant temporal and spatial scales. The grid resolution and the different grid sizes, $N_{\Delta x}$, are provided in Table 1. The computational meshes ensure that the wide range of turbulent scales are well resolved with grid spacing close to $\Delta y^+ = 1$. The radial, azimuthal and streamwise grid spacings are reported in y⁺-units and different ranges are provided because the mesh varies within the computational domain. Note that the skin friction values used to calculate the grid spacings in y⁺-units were obtained from non-rotating turbulent pipe flow simulations. Hence, the provided grid spacings in y⁺units are conservative estimates for the rotating pipe flow simulations because the skin friction values are expected to be lower for a rotating pipe due to the expected turbulence suppression. To obtain fully-converged turbulent statistics,

a total compute time of at least ten flow-through times is used, which does not include the initial transient time covering a small fraction of the compute time.

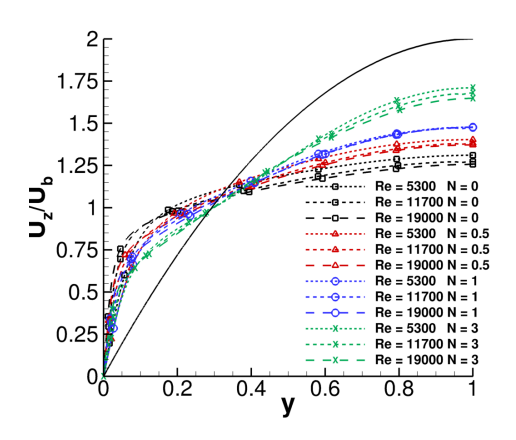
Table 1. Details of turbulent pipe flow simulations assuming a streamwise extend of 15D, where Re refers to Reynolds number, Δr^+ , $\Delta R\Theta^+$ and Δz^+ are the grid spacings measured in y^+ -units and $N_{\Delta x}$ is the number of grid points in the computational domain. Note that for the grid spacings different ranges are provided because the mesh is non-uniform.

Re	$\Delta r^+/\Delta R\Theta^+/\Delta z^+$	$N_{\Delta x} \times 10^6$
5,300	0.14-4.4/1.5-4.5/3.0-9.9	20
11,700	0.16-4.7/1.5-5.0/3.0-9.9	120
19,000	0.15-4.5/1.5-4.8/3.0-10.	440

The mesh is comprised of hexahedral elements with the solution being composed of Nth-order tensor product polynomials within each element. Local lexicographical ordering within each macro element, and the need to evaluate only $\mathcal{O}(EN^4)$ discrete operators, which typically have $\mathcal{O}(EN^6)$ non-zeros, leads to the cache and vectorization efficiency (Fischer *et al.* (2008)). Nek5000 minimally uses external libraries to increase compile speed, and matrix operations are implemented in assembler code M×M routines to speed up computations. Furthermore, Nek5000 tests each of the three parallel algorithms at the beginning of each run to determine which behaves optimally thus parallelism is automatically tuned for each machine. The algebraic multigrid solver was chosen throughout this work from the different pressure Poisson solvers available in Nek5000.

3 EFFECTS ON MEAN FLOW

The streamwise velocity profiles as shown in Fig. 2a illustrate how the turbulent flow is affected by rotation in the mean. The velocity profiles are plotted versus the distance from the wall y = 1 - r/R where r is the local radius and Ris the total radius of the pipe. It can be seen that the streamwise velocity profile tends towards the laminar profile as the rotation number N is increased. Near the wall the wallnormal velocity gradient is reduced which leads to a reduction in skin friction and a speed up of the flow towards the center of the pipe. It can be noticed that the velocity profile for all Reynolds numbers and rotation numbers cross each other at around the same y-location ($y \approx 0.4$). Figure 2b displays mean swirl velocity profiles for the different Reynolds and rotation numbers. Orlandi & Fatica (1997) previously observed the occurrence of the same inflection point in the velocity profiles as observed in Figure 2b and they noticed that the inflection point (at $y \approx 0.4$) appears to coincide with the location where the mean streamwise vorticity $\langle \omega_z \rangle$ is zero (or the mean swirl $r < v_{\Theta} >$ has an extrema). The location of the extrema in the mean swirl profiles appear to shift towards the wall with increasing rotation number whereby some Reynolds number dependence appears to present. As pointed out in Ref. 15, Eggels et al. (1994) showed that $\langle v_{\Theta} \rangle$ should be a linear function of the radial position r and proportional to r^2 towards the center. The mean flow



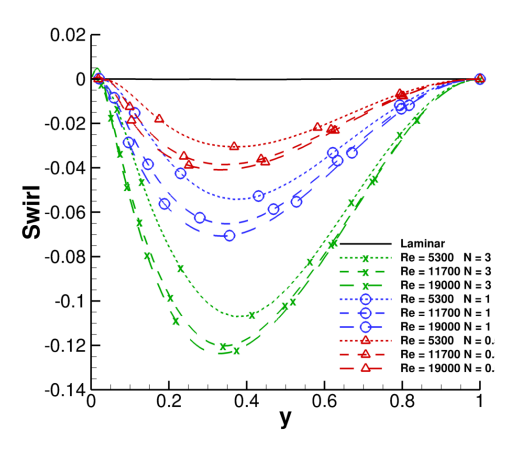


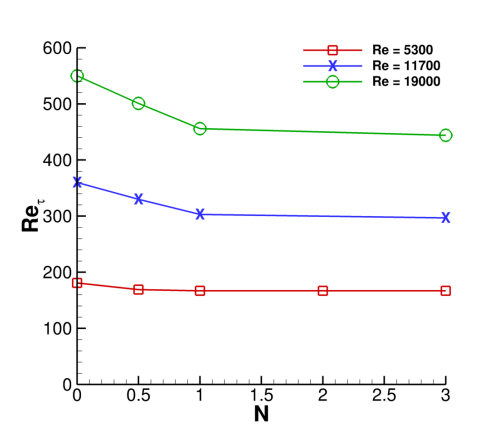
Figure 2. (a) Mean stream-wise velocity profiles normalized by the bulk velocity and (b) swirl velocity profiles for different Reynolds and rotation numbers.

quantities of the present results are generally in good agreement with prior numerical and experimental results Orlandi & Fatica (1997, 1998); Reich & Beer (1989); Kikuyama *et al.* (1983); Orlandi & Ebstein (2000); Orlandi & Fatica (1998).

As the mean velocity profiles demonstrated, rotation leads to a reduction in near wall gradient and, therefore, reduction in skin friction or friction velocity u_{τ} defined as $\sqrt{\tau_w/\rho}$, where τ_w is the wall shear stress and ρ is the fluid density. Figure 3a shows the behavior of the friction Reynolds number $Re_{\tau} = u_{\tau}D/v$ with respect to the rotation number N for the three different Reynolds numbers considered in this study. Due to the reduction in wall shear stress the friction velocity drops significantly as soon as the flow is rotated. In order to gauge the relative reduction, Figure 3b displays the friction Reynolds number normalized by the non-rotating friction Reynolds number. A significant drop off in the friction Reynolds number can be observed up to a rotation number of N=1 for Re=11,700 and Re=19,000and up to N=0.5 for Re=5,300. Orlandi & Fatica (1997) conducted DNS at a low Reynolds number of Re=4,900 and had speculated about possible Reynolds number effects. The results shown here clearly demonstrate that Reynolds number effects can be observed in the mean flow characteristics as well as in the turbulent statistics discussed later. The trend displayed in Figure 3b with a rapid reduction in friction Reynolds for low rotation numbers and a seemingly saturation for larger rotation numbers (within the range of the data set) suggests that rotation loses its effectiveness in reduction of near-wall wall-normal velocity gradients or

skin friction at larger rotation numbers. It should be noted that further simulations are needed to obtain a better understanding about the transition between the two regimes in the vicinity of N=1.

Simply considering the extrema of the effects of rotation on purely laminar flows may provide some idea on the abrupt change in the effectiveness of rotation on skin friction reduction. It is well-known that while the parabolic pipe flow profile (N=0) is linearly stable, additional rotation causes a destabilization of the flow. On the other hand, when considering the extreme case of a purely rotating laminar flow $(N \to \infty)$ inside a cylinder, adding crossflow causes a destabilization of the canonical flow. Hence, $N \approx 1$ potentially provides the boundary between these two regimes.



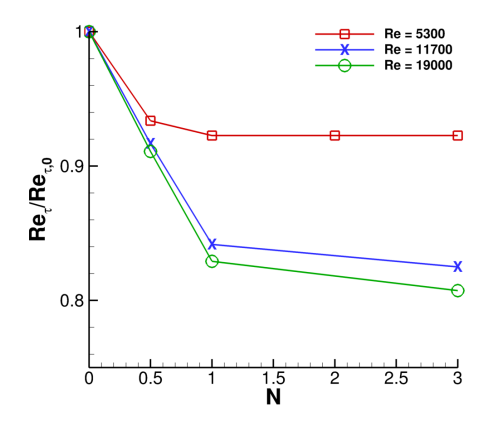


Figure 3. (a) Friction Reynolds number Re_{τ} versus rotation number N for different Reynolds numbers. (b) Friction Reynolds number normalized by non-rotating friction Reynolds number.

4 QUANTIFYING TURBULENCE SUPPRES-SION

Before diving into the analysis of the characteristics of the turbulent flow, the goal is to quantify turbulence suppression in rotating pipe flows, as many prior works have simply stated its presence but have not clearly quantified. A good starting point for quantifying turbulence suppression is to compute the turbulent kinetic energy and normalize it by the bulk velocity (see Figure 4a). For the sake of brevity,

only the results for Re=19,000 are shown. As commonly done in prior studies, only the streamwise bulk velocity, U_b , is considered here for normalization. The plots of turbulent kinetic energy normalized by the streamwise velocity squared display two clear trends. The peak turbulent kinetic energy in the vicinity of the wall is reduced with increasing rotation number and the values away from the wall are increased. When considering turbulent kinetic energy in inner scale the near wall peak stays fairly constant and the increase in turbulent kinetic energy towards the center is more emphasized (not presented here, see Davis et al. (2019) for more details). In order to determine if turbulence suppression occurs, the mean turbulent kinetic energy was integrated over the circular cross-section of the pipe and is displayed in Figure 4b. For Re=11,700 and 19,000, the total kinetic energy (TKE) initially reduces and increases for larger rotation numbers. Within the range of the available data in this DNS study, a change in the trends can clearly be observed at around $N \approx 1$. The results shown in Figure 4b do not generally point towards turbulence suppression for these flows.

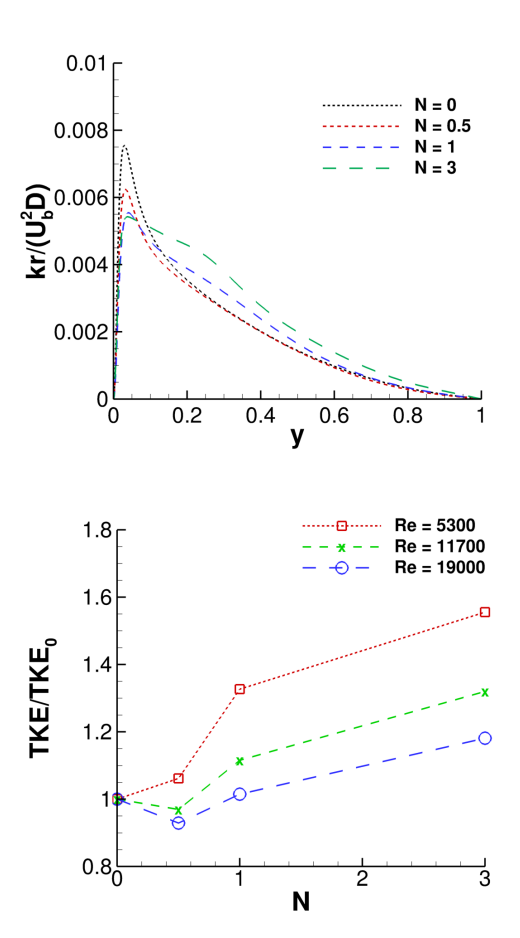


Figure 4. (a) Turbulent kinetic energy normalized by bulk streamwise velocity squared and compensated with radius and (b) total turbulent kinetic energy normalized by total mean streamwise velocity squared.

The first objection towards the way the data is represented in Figure 4b (as was done in many prior works) is that the mean kinetic energy contribution from the added mean azimuthal velocity component to the total mean kinetic energy must also be considered. Figure 5a displays the turbulent kinetic energy versus wall distance compensated

by the local radius (accounting for the area contribution in the integrand) and normalized with the total mean kinetic energy $(TKE^*=1/2(<V_z>^2+<V_{\Theta}>^2)A)$. A clear reduction in turbulent kinetic energy can be observed throughout the cross-section for Re=19,000. The total kinetic energy for all three Reynolds numbers versus rotation number is illustrated in Figure 5b and a reduction in turbulent kinetic energy was obtained for all rotation numbers at Reynolds numbers of Re=11,700 and 19,000. Interestingly, an initial increase in turbulent kinetic energy can still be observed until N=1 for Re=5,300 and, thus, considering turbulence being suppressed may not appropriately describe the characteristics of this flow at these conditions. It can be summarized that turbulence suppression is occurring (for large enough rotation numbers) for all three Reynolds numbers used in this study. As previously observed, the results for the turbulent kinetic energy also display a seemingly change in trends at N=1 for all three Reynolds numbers.

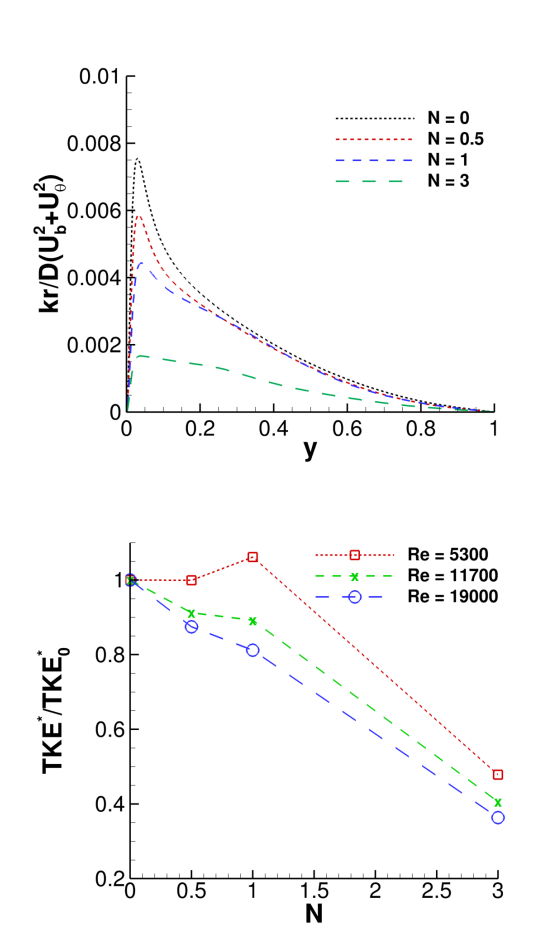


Figure 5. (a) Turbulent kinetic energy normalized by bulk velocity magnitude squared and compensated with radius, and (b) total turbulent kinetic energy normalized by total mean velocity magnitude squared.

5 REYNOLDS STRESS TENSOR

In the following discussion the focus will be on the largest Reynolds number case where it has been established in the foregoing discussion that turbulence suppression as quantified in Figure 5b is occurring for all rotation numbers. While rotation is leading to an overall reduction in

turbulent kinetic energy normalized with the mean kinetic energy, another important effect of rotation is that it causes a reorganization of the turbulence. The characteristics of this flow are further analyzed by considering the different structure of the Reynolds stress tensor. Figures 6a-c show the inner-scaled Reynolds stress tensor components for different rotation numbers. The Reynolds stress tensor was rotated in the local streamline-aligned coordinate system, where $\langle u_1 u_1 \rangle^+$ is the normal Reynolds stress aligned with the streamline direction, $\langle u_2 u_2 \rangle^+$ is aligned with the radial direction, and $\langle u_3 u_3 \rangle^+$ is the normal Reynolds stress in the direction orthogonal to the other two. Rotation causes a significant reduction in the magnitude of the near wall peak in $\langle u_1 u_1 \rangle^+$. Furthermore, at larger rotation numbers this narrow peak typically observed at $y^+ \approx 15$ for pipe flows becomes much wider and reaches a maximum further from the wall. Note that in Davis et al. (2019) it is shown that rotation prevents the formation of a typical log-layer. The normal stress in the radial direction shows a consistent trend with increasing N in the form of an increased magnitude towards the center of the pipe. For N=3, a second peak slightly exceeding the magnitude of the inner peak appears near the pipe centerline. Close to the wall, the u_3 direction, and hence the normal Reynolds stress $\langle u_3u_3\rangle^+$, is closely aligned with the azimuthal direction. For N>0, this component of the Reynolds stress tensor displays a narrow peak similar to that typically observed in the streamwise direction for N=0. In addition to this narrow peak, the N=3case also shows the formation two additional peaks, i.e., one around the same location where the main peak in $\langle u_1 u_1 \rangle^+$ is occurring and a second peak appears to establish itself towards the center. It should be noted that these types of peaks have been observed in previous works and are not an artifact of insufficient time-averaging.

Another way to examine the Reynolds stress tensor is to compute the eigenvalues and eigenvectors (or principle values and axes). An advantage of transforming the Reynolds stress tensor into its principal axes is that the N>0 cases can more closely be compared to the Reynolds stresses for the N=0 case since the general shape for the principal values versus local radius keeps some of features observed for the N=0 case. Figure 7a shows the three eigenvalues $\sigma_1 > \sigma_2 > \sigma_3 > 0$ (not normalized) for the rotating and non-rotating turbulent flows. For all Reynolds numbers, a narrow near wall peak can be observed for σ_1 . As the rotation number increases, a second peak establishes towards the center of the pipe. The principal values σ_2 and σ_3 show a similar trend to the N=0 case where the inner peak is slightly reduced (except for σ_2 at N=3) and larger values are obtained towards the center of the pipe. In general, rotation has the tendency to redistribute turbulent fluctuations (more evenly) over the cross-section. In addition to the principal values, we also extracted the orientation of the principal axes by computing the angles ϕ_{rz} and $\phi_{r\Theta}$ about the Θ and z axes in the (r,z) and (r,Θ) -planes, respectively. A reorientation of the principal axes of the Reynolds stress tensor can clearly be observed in Figures 7b and 7c. For the non-rotating pipe, the second principle axes is aligned with the Θ -direction. For the rotating pipe flow cases, with increasing y the principal axes start to deviate away the directions observed for the non-rotating pipe flow. While the N = 0.5 case only shows a mild variation away from these directions with increasing rotation number the change in the orientation (especially towards the center) becomes very significant. Overall, a significant reorientation of the

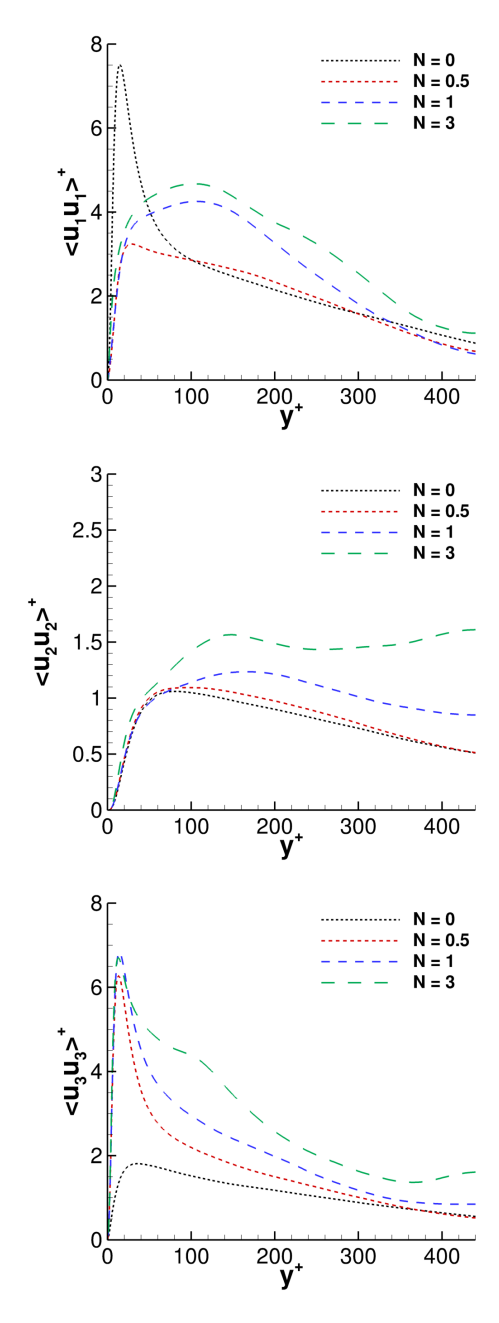


Figure 6. Streamline aligned normal Reynolds stresses normalized by u_{τ}^2 for Re=19,000.

Reynolds stress tensor can be observed for the rotating pipe flow in comparison with the stationary pipe.

6 PRODUCTION AND DISSIPATION TERMS

Finally, turbulent kinetic energy budgets for these flows are calculated (only dissipation and production are shown here). The budgets were compared with existing data by El Khoury *et al.* (2013) for a non-rotating pipe and lower Reynolds number results for the rotating pipe to validate the simulation approach (see Davis *et al.* (2019) for details). Figures 8a and 8b show a strong reduction in (nonnormalized) turbulence production and a decrease in dissipation at the wall. Rotation about the center axis and the presence of the centrifugal force inhibits the wall-normal momentum exchange which in turn will reduce the nearwall gradients. Ultimately, the reduction in turbulence pro-

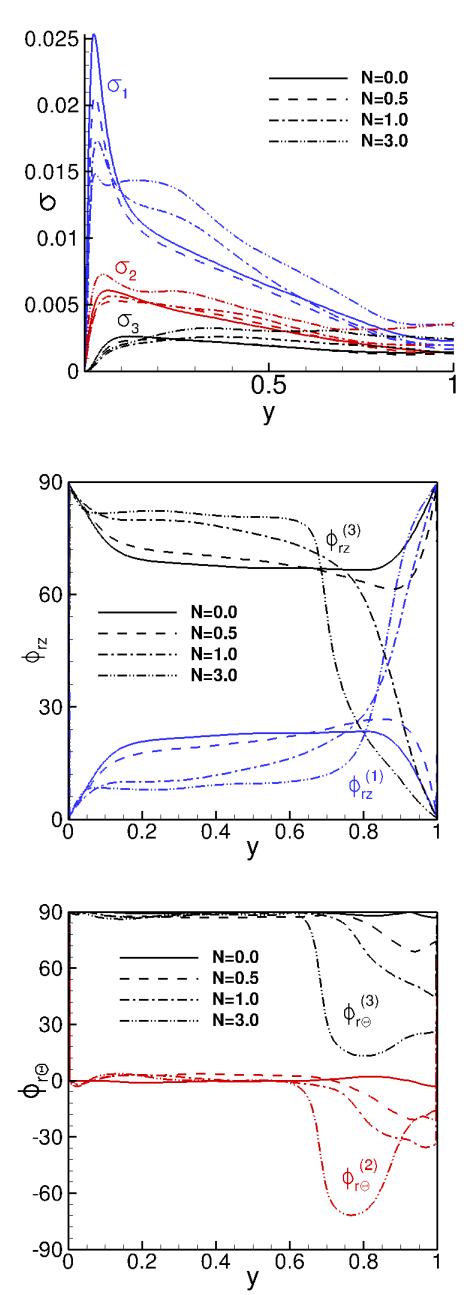


Figure 7. (a) Principal values σ_i of Reynolds stress tensor and (b,c) orientation angle of principle axes.

duction can be attributed to a reduction in the near wall gradients. The insets in Figures 8a and 8b display the dissipation and production terms in inner scales, i.e., normalized with the friction velocity. The normalized turbulent production terms (Fig. 8a) are not significantly affected by rotation; however, exhibit some mild increase towards the center of the flow that is much less evident in studies conducted at lower Reynolds numbers. The increased normalized dissipation for the rotating pipe cases near the wall shown in Fig. 8b is consistent with observations by Orlandi & Fatica (1997). The increased (normalized) dissipation close to the wall and production far from the wall contribute to the formation of what has been described previously by Orlandi & Fatica (1997) as a plateau in some of the normal Reynolds stresses far from the wall, but investigation at higher Reynolds numbers shows this to appear as a second peak. Further investigations at higher Reynolds

numbers are currently being performed to determine the effects of rotation on turbulent pipe flows at a larger range of Reynolds numbers.

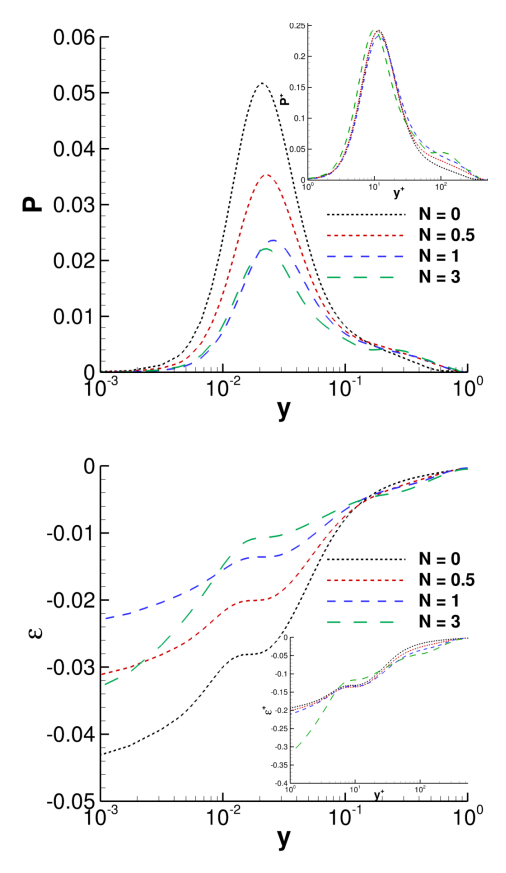


Figure 8. (a) Dissipation and (b) production terms in outer and inner scales for different rotation numbers N at a Reynolds number of Re = 19,000.

7 CONCLUSION

In summary, DNS of rotating pipe flows have been performed at larger Reynolds numbers than previously published. The results showed a significant reduction in skin friction as previously reported for lower Reynolds numbers whereby significant Reynolds number effects could be observed in the range of Reynolds numbers considered. One of the main objectives in this work was to quantify the occurrence of turbulence suppression in rotating flows. When computing the total turbulent kinetic energy and normalizing it by the mean kinetic energy (including the contribution from the azimuthal velocity component) turbulence suppression could be identified for all Reynolds numbers and large enough rotation numbers. Interestingly, the lower Reynolds number case did not show a reduction in relative turbulent kinetic energy for all rotation numbers. The rotating turbulent pipe flow was observed to change some characteristics, such as the efficiency in skin friction reduction, around $N \approx 1$ but further analysis is needed to substantiate these initial findings. The analysis of the Reynolds stress tensor showed that the Reynolds stress components are significantly affected by the presence of rotation in the flow which was found to be consistent with prior work. In addition, it was demonstrated that a reorientation of the principle axes of the Reynolds stress tensor could be observed.

REFERENCES

- 52.
- Ashton, N., Davis, J. & Brehm, C. 2019 Assessment of the elliptic blending reynolds stress model for a rotating turbulent pipe flow using new dns data. In AIAA Aviation and Aeronautics Forum and Exposition Dallas, TX, June 17 to June 21, AIAA Paper 2019.
- Davis, J., Ganju, S., Bailey, S. & Brehm, C. 2019 A dns study to investigate turbulence suppression in rotating pipe flows. In AIAA Aviation and Aeronautics Forum and Exposition Dallas, TX, June 17 to June 21,. AIAA Paper 2019.
- Eggels, JGM, Boersma, BJ & Nieuwstadt, FTM 1994 Direct and large eddy simulations of turbulent flow in an axially rotating pipe. Unpublished, results shown in Eggels 1994.
- El Khoury, George K, Schlatter, Philipp, Noorani, Azad, Fischer, Paul F, Brethouwer, Geert & Johansson, Arne V 2013 Direct numerical simulation of turbulent pipe flow at moderately high reynolds numbers. *Flow, turbulence and combustion* **91** (3), 475–495.
- Facciolo, Luca, Tillmark, Nils, Talamelli, Alessandro & Alfredsson, P Henrik 2007 A study of swirling turbulent pipe and jet flows. *Physics of Fluids (1994-present)* 19 (3), 035105.
- Feiz, AA, Ould-Rouis, M & Lauriat, Guy 2005 Turbulence statistics in a fully developed rotating pipe flow. *Journal* of Enhanced Heat Transfer 12 (3).
- Fischer, P.F., Lottes, J.W. & Kerkemeier, S.G. 2008 Nek5000, http://nek5000.mcs.anl.gov.
- Imao, Shigeki, Itoh, Motoyuki & Harada, Takeyoshi 1996 Turbulent characteristics of the flow in an axially rotating pipe. *International Journal of Heat and Fluid Flow* 17 (5), 444–451.
- Kikuyama, Koji, Murakami, Mitsukiyo, Nishibori, Kenji & Maeda, Kazuhiko 1983 Flow in an axially rotating pipe: A calculation of flow in the saturated region. *Bull. JSME* 26 (214), 506–513.
- Murakami, Mitsukiyo & Kikuyama, Kouji 1980 Turbulent flow in axially rotating pipes. *Journal of Fluids Engi*neering 102 (1), 97–103.
- Nishibori, Kenji, Kikuyama, Koji & Murakami, Mitsukiyo 1987 Laminarization of turbulent flow in the inlet region of an axially rotating pipe. *JSME International Journal* **30** (260), 255–262.
- Oberlack, Martin 1999 Similarity in non-rotating and rotating turbulent pipe flows. *Journal of Fluid Mechanics* **379**, 1–22.
- Oberlack, Martin 2001 A unified approach for symmetries in plane parallel turbulent shear flows. *Journal of Fluid Mechanics* 427, 299–328.
- Orlandi, Paolo & Ebstein, David 2000 Turbulent budgets in rotating pipes by dns. *International Journal of Heat and Fluid Flow* **21** (5), 499–505.
- Orlandi, Paolo & Fatica, M 1997 Direct simulations of turbulent flow in a pipe rotating about its axis. *Journal of Fluid Mechanics* **343**, 43–72.
- Orlandi, P & Fatica, M 1998 Direct simulations of turbulent flow in a pipe rotating about its axis. *Oceanographic Literature Review* **7** (45), 1257.
- Reich, G & Beer, H 1989 Fluid flow and heat transfer in an axially rotating pipei. effect of rotation on turbulent pipe flow. *International Journal of Heat and Mass Transfer* 32 (3), 551–562.
- White, A 1964 Flow of a fluid in an axially rotating pipe. Journal of Mechanical Engineering Science 6 (1), 47–